J|A|C|S COMMUNICATIONS

Published on Web 12/10/2010

Low Reflectivity and High Flexibility of Tin-Doped Indium Oxide Nanofiber Transparent Electrodes

Hui Wu,[†] Liangbing Hu,[†] Thomas Carney,[†] Zhichao Ruan,[‡] Desheng Kong,[†] Zongfu Yu,[‡] Yan Yao,[†] Judy J. Cha,[†] Jia Zhu,[‡] Shanhui Fan,[‡] and Yi Cui*[,†]

Departments of Materials Science and Engineering and Electrical Engineering, Stanford University, Stanford, California 94305, United States

Received October 13, 2010; E-mail: yicui@stanford.edu

Abstract: Tin-doped indium oxide (ITO) has found widespread use in solar cells, displays, and touch screens as a transparent electrode; however, two major problems with ITO remain: high reflectivity (up to 10%) and insufficient flexibility. Together, these problems severely limit the applications of ITO films for future optoelectronic devices. In this communication, we report the fabrication of ITO nanofiber network transparent electrodes. The nanofiber networks show optical reflectivity as low as 5% and high flexibility; the nanofiber networks can be bent to a radius of 2 mm with negligible changes in the sheet resistance.

Transparent conducting oxides (TCOs) are of fundamental interest for the modern electronics industry because of the necessity of transparent electrodes in devices such as displays, organic light-emitting diodes (OLEDs), thin-film transistors (TFTs), and solar cells.[1] Tin-doped indium oxide (ITO) is the most commonly used TCO layer because of its high conductivity and high transmittance.[2,3] Although there has been much success after 60 years of research and development, two significant problems with ITO still remain.[2,4] The first is ITO's poor flexibility, which severely limits it for applications in flexible and stretchable electronics.[4,5] The second is its strong reflection of light. ITO's index of reflection is ∼2.0, leading to a total reflection of ∼10% from a single side. Such high reflection leads to problems for certain applications. For example, in touch screens, two layers of ITO are layered on top of one another, regrettably producing a final total reflection of 20%.[6] Such directional reflection is a major problem for devices operating in bright environments.[7]

To solve these two problems, we designed and fabricated ITO nanofiber networks using electrospinning, a quick, effective technique that produces continuous nanofiber webs.[8] For transparent electrode applications, one clear advantage of electrospun nanofibers is their large aspect ratios, which result in an extraordinarily low percolation critical density. ITO nanofibers synthesized by electrospinning were first reported by Pan and co-workers[9] and Munir et al.;[10] however, the conductivity in their structures was too low (conductivity of ∼1 S/cm for a single nanofiber or a sheet resistance of >1 MΩ/sq for nanofiber thin films), making it useful only for antistatic applications. In this study, a 100-fold higher conductivity in an electrospun ITO nanofiber was achieved by using different precursors and subsequent doping during the heat treatment processes (see the experimental details in the Supporting Information). Figure 1a,b shows scanning electron microscopy (SEM) and transmission electron microscopy (TEM) images of electrospun ITO nanofibers demonstrating that the synthesized nanofibers are continuous with diameters of 80 ± 20 nm and surface roughness of <10 nm. No pores can be seen in the fibers in the SEM and TEM images, suggesting that the fibers are dense. The selected-area electron diffraction (SAED) pattern and the high-resolution TEM (HRTEM) image (insets of Figure 1b) revealed the ITO nanofibers to be polycrystalline with grain sizes of roughly 8 nm. The chemical composition of individual nanofibers was determined by energy-dispersive X-ray spectroscopy (EDS) (Figure S1 in the Supporting Information), which revealed the In/Sn ratio to be ∼9:1. From X-ray diffraction (XRD) analysis (Figure S2), the crystal structure of the nanofibers was determined to be the cubic bixbyite In_2O_3 structure, and no other phases corresponding to tin compounds were detected. Thus, we can conclude that the Sn is in a solid solution with In_2O_3. In addition, the work function of ITO nanofibers was measured by photoemission yield spectroscopy in air (Figure S3) and found to be 4.9 eV, consistent with values reported in the literature[11] and ideal for providing hole injection/extraction contacts in OLED displays and organic solar cells.

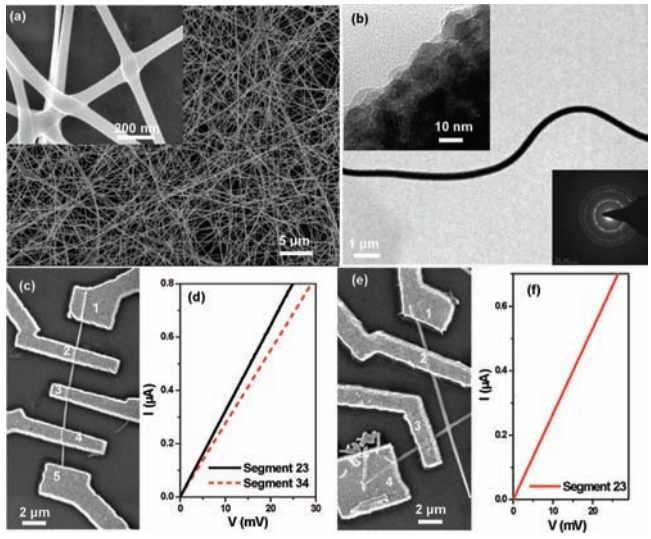

Figure 1. (a) SEM images of synthesized ITO nanofibers. (b) TEM image of an ITO nanofiber. Upper inset: HRTEM image. Lower inset: SAED pattern. (c, d) Electrical conductivity measurement on a single ITO nanofiber. (e, f) Electrical conductivity measurement on two crossed ITO nanofibers.

The electrical transport properties of the ITO nanofibers were studied using four-point-contact devices on individual nanofibers to measure their current−voltage ($I-V$) characteristics. ITO nanofibers were transferred to an oxidized silicon substrate (300 nm SiO_2/Si) for device fabrication by sonicating the fiber network in methanol for ∼1 min and drop-casting the solution onto the substrate. After a suitable nanofiber was located, standard electron-

[†] Department of Materials Science and Engineering.
[‡] Department of Electrical Engineering.

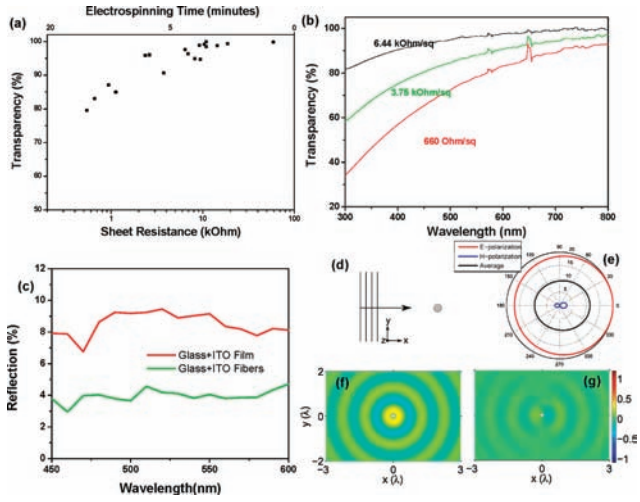

Figure 2. (a) Transmittance at 550 nm vs sheet resistance for ITO nanofiber networks deposited with different electrospinning times. (b) Transmittance spectrum of ITO nanofiber networks with different sheet resistances. (c) Reflection of an ITO nanofiber and sputtered ITO thin film on glass. (d−g) Optical simulation of light scattering on ITO nanofibers: (d) Schematic of the scattering of a nanofiber. (e) Polar diagram of the angular scattering intensity. The unit of the radial axis is nm/radian. (f, g) Scattering field distributions for the (f) *E* polarization and (g) *H* polarization.

beam lithography followed by thermal evaporation of a Cr/Au (5 nm/200 nm) film was used to create multiple ohmic electrodes for the transport study. *I*−*V* measurements on nanofiber devices were performed using the standard four-terminal configuration, in which a current is supplied from the outermost electrodes and the voltage drop between the two inner electrodes is measured in order to minimize the contact resistance. To ensure that the linear resistance was uniform along the nanofiber, multiple electrodes were placed along the nanofiber. The two inner segments exhibited similar properties, corresponding to conductivity values of 4500 S m^{-1} (segment 2−3) and 4300 S m^{-1} (segment 3−4) (Figure 1c,d). Although the conductivity of individual ITO nanofibers was slightly lower than that of those created with the high-vacuum deposition process[12] or chemical vapor deposition (CVD),[13] it is better than that of sol−gel films.[14] Moreover, we managed to fabricate a device across a junction of two nanofibers. As shown in Figure 1d, the linear *I*−*V* relation proved the junction to be ohmic in nature, without a detectable energy barrier that would have limited the electron transport. The average conductivity of the nanofiber between the two inner electrodes was 5200 S m^{-1} (Figure 1e,f), indicating a negligible junction resistance. This observation is not surprising, since during the annealing process, the ITO nanofibers fuse together entirely at the junction (Figure 1a inset). Highly conductive and reliable junctions are essential for the electrical properties of nanofiber network, in which innumerable fiber crossings occur. The fused junctions between fibers also enhance the mechanical integrity of nanofiber webs, as will be discussed later.

We measured the sheet resistance and optical transmittance of ITO nanofiber networks. As shown in Figure 2a, the resistance and transparency of ITO nanofiber films can be controlled by the electrospinning deposition time. For a time of 3 min, for example, the transparency was 96% and the sheet resistance 10 kΩ/sq. As the electrospinning time increased, the density of nanofiber per area grew, resulting in reduced transparency and a lower sheet resistance. As shown in Figure 2a, a minimum sheet resistance of 660 Ω/sq was achieved at ∼80% transparency. Decreasing the fiber diameter by reducing the precursor concentration in the electrospun solutions[8] may further increase the transparency of nanofiber mats. The transmittances for ITO nanofiber films having several different densities are shown in Figure 2b. The UV absorption edge was located at ∼300 nm, which is equivalent to a photon energy of 4.14 ± 0.02 eV.[2]

The rough surface of the ITO nanofiber networks enhanced the diffusive light scattering and decreased the directional reflection of light. Directional reflections of ITO nanofibers and an ITO film on glass were measured using light incident from the glass side to simulate the real application situation. Figure 2c shows the directional reflection data at different wavelengths. On average, the directional light reflection was ∼9% for the ITO thin film on glass and ∼3.5% for the ITO nanofiber network on glass. This lower reflection of the nanofiber network can be attributed into two factors. First, the nanofiber network generally has a lower effective refractive index than a pure ITO thin film because air occupies voids in the nanofiber network. Therefore, the total reflection, including directional and diffusive components, is substantially reduced. Second, the directional reflection is reduced because the nanofiber network can diffuse light more effectively than a flat film. To understand this point, we simulated the scattering of a single nanofiber using the Lorentz−Mie method.[15] For a plane wave with a wavelength of 550 nm impinging normally upon the nanofiber from the left side (Figure 2d), the angular scattering intensity was calculated and is shown in Figure 2e. When the plane wave is *E*-polarized with the electric field parallel to the fiber, the scattering field is generated by the induced parallel electric dipole, which gives an isotropic scattering pattern in all in-plane directions. (Figure 2f). In contrast, for *H* polarization with the magnetic field parallel to the fiber, the incident wave has the electric field in the *y* direction and excites a scattering field dominated by a *y*-direction electric dipole, which shows directional scattering (Figure 2g). However, the strength of this directional scattering is much weaker, so the scattering intensity for the unpolarized light, which averages over the *E* and *H* polarizations, is mostly isotropic (Figure 2e). As a result, these ITO nanofibers, when arranged with random orientations in a three-dimensional network, lead to diffusive scattering and hence reduce the directional reflection.

In addition to being conductive and transparent, electrodes in the next generation of optoelectronic devices must be flexible. This requirement severely limits the use of traditional ITO thin films as transparent conductors because dense ITO films fail under bending. Inorganic nanomaterials with a one-dimensional configuration have been demonstrated to have high flexibilities.[16] The SEM images in Figure 3a,b show the great flexibility of the ITO nanofiber networks. A free-standing nanofiber film can easily be bent to a radius of less than 100 μm without any fractures (Figure 3b). Moreover, it can be observed that after bending, the nanofibers do not lose contact with one other because of their fused junctions. In comparison, sputtered ITO films begin to break at a bending radius of 10 mm (parallel cracks form in the ITO film after bending[3,4]). Figure 3c plots the results of static resistance tests on an ITO nanofiber network coated on a poly(ethylene terephthlate) (PET) film and an ITO thin film sputtered onto PET after bending to different radii. The resistance of the sputtered ITO thin film increased abruptly after bending to a radius below 10 mm because of the formation of cracks in the ITO films, which break the conduction path for the free carriers. In contrast to the dense ITO films, the ITO nanofiber network on PET kept its structural integrity after being bent to a radius as low as 1 mm. The increase in sheet resistance after the film was bent to a radius of 1 mm was 16% for the ITO nanofibers and 3400% for the ITO thin film. Figure 3d shows the resistance changes of ITO nanofibers and thin films after

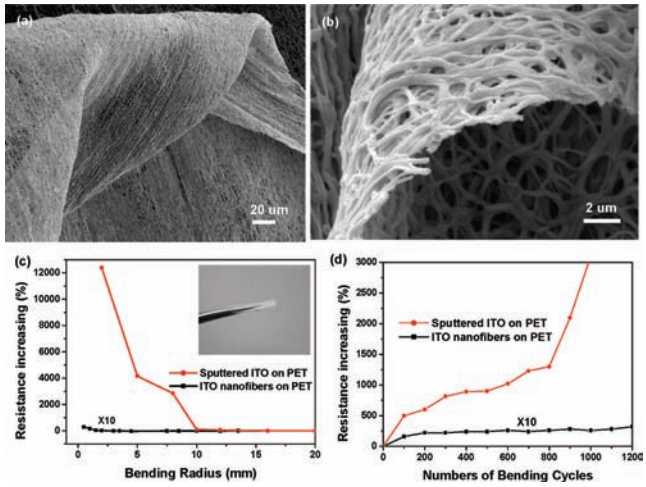

Figure 3. (a)-(b) SEM images of freestanding ITO nanofiber webs after bending, showing superior flexibility of ITO nanofibers. (c)-(d) Resistance change of PET coated with ITO nanofibers and sputtered ITO films with bending test: (c) after bended to different radius, (d) after bended to 10 mm radius for different times. Inset of (c) shows digital photo of ITO nanofiber coated PET film after bending.

repeated dynamic bending tests. A significant difference between the electrical resistances of the ITO nanofibers and thin films was also observed. The electrical resistance increased sharply by a factor of 10 000 in the case of the ITO films after the first 100 cycles. In contrast, the electrical resistance of the ITO nanofibers increased only 30% even after more than 1000 bending cycles. This finding further confirms the mechanical flexibility of the ITO nanofibers, indicating that ITO nanofibers are more durable over bending cycles, making them suitable for modern applications such as touch screens.

In summary, ITO nanofibers have been synthesized by electrospinning. Because of the high aspect ratio of ITO nanofibers and fused junctions between them, high transparency, low resistance, and excellent mechanical flexibility have been achieved. There was no observable change in conductivity after the film was bent to a radius of 2 mm, which is superior to the performance of flat ITO films on plastic substrates. Because of the rough surface of the ITO nanofiber network, the light scattering was more dramatic than that from flat ITO films, as confirmed by experimental data and modeling. Such highly transparent, much less reflective, flexible ITO nanofiber-based electrodes are sure to be used in novel applications.

Acknowledgment. Y.C. acknowledges support by a King Abdullah University of Science and Technology (KAUST) Investigator Award (KUS-l1-001-12) and the U.S. Department of Energy. S.F. acknowledges support from the U.S. Department of Energy (DE-FG02-07ER46426).

Supporting Information Available: Synthesis and characterization methods, EDS spectrum, XRD pattern, and photoemission yield spectrum. This material is available free of charge via the Internet at http://pubs.acs.org.

References

(1) Minami, T. *Thin Solid Films* **2008**, *516*, 5822–5828.
(2) Granqvist, C. G.; Hultaker, A. *Thin Solid Films* **2002**, *411*, 1–5.
(3) Chopra, K. L.; Major, S.; Pandya, D. K. *Thin Solid Films* **1983**, *102*, 1–46.
(4) Kumar, A.; Zhou, C. W. *ACS Nano* **2010**, *4*, 11–14.
(5) Sun, Y. G.; Rogers, J. A. *Adv. Mater.* **2007**, *19*, 1897–1916.
(6) Hecht, D. S.; Thomas, D.; Hu, L. B.; Ladous, C.; Lam, T.; Park, Y.; Irvin, G.; Drzaic, P. *J. Soc. Inf. Disp.* **2009**, *17*, 941–946.
(7) *Flexible Flat Panel Displays*; Crawford, G. P., Ed.; Wiley Series in Display Technology; Wiley: Chichester, England, 2005.
(8) Li, D.; Xia, Y. N. *Adv. Mater.* **2004**, *16*, 1151–1170.
(9) Lin, D.; Wu, H.; Zhang, R.; Pan, W. *Nanotechnology* **2007**, *18*, 465301.
(10) Munir, M. M.; Iskandar, F.; Yun, K. M.; Okuyama, K.; Abdullah, M. *Nanotechnology* **2008**, *19*, 145603.
(11) Schlaf, R.; Murata, H.; Kafafi, Z. H. *J. Electron Spectrosc. Relat. Phenom.* **2001**, *120*, 149–154.
(12) Kim, H.; Pique, A.; Horwitz, J. S.; Mattoussi, H.; Murata, H.; Kafafi, Z. H.; Chrisey, D. B. *Appl. Phys. Lett.* **1999**, *74*, 3444–3446.
(13) Wan, Q.; Dattoli, E. N.; Fung, W. Y.; Guo, W.; Chen, Y. B.; Pan, X. Q.; Lu, W. *Nano Lett.* **2006**, *6*, 2909–2915.
(14) Prodi-Schwab, A.; Luthge, T.; Jahn, R.; Herbig, B.; Lobmann, P. *J. Sol-Gel Sci. Technol.* **2008**, *47*, 68–73.
(15) Hulst, H. C. v. d. *Light Scattering by Small Particles*; Dover: New York, 1981.
(16) Ju, S. Y.; Facchetti, A.; Xuan, Y.; Liu, J.; Ishikawa, F.; Ye, P. D.; Zhou, C. W.; Marks, T. J.; Janes, D. B. *Nat. Nanotechnol.* **2007**, *2*, 378–384.

JA109228E